A One-Component, Magnetic Support-and-Balance System

KENNETH R. SIVIER*
University of Illinois, Urbana, Ill.

A one-component, magnetic support-and-balance system was designed and built as part of a wind-tunnel investigation of sphere drag at subsonic Mach numbers and Reynolds numbers in the range from about 25 to several thousand. This experimental approach has two important advantages: 1) the tests are free of the effects of model support interference and 2) the balance sensitivity increases as the model size is decreased to obtain lower Reynolds numbers. The magnetic system was used with a vertical wind tunnel, permitting the alignment of the drag and gravity force and the use of a true one-component support. The use of the system proved to be simple and effective under those flow conditions for which negligible lateral aerodynamic forces exist. With $\frac{1}{16}$-in.-diam spheres, drag measurements were made at values of *Re* down to about 25; the corresponding drag force was about 4 mg. Under flow conditions where substantial unsteady, lateral forces exist, the natural radial magnetic restraint was insufficient to prevent significant lateral motion of the model. In spite of this motion, it was possible to obtain good drag data at Reynolds numbers up to about 4000.

Nomenclature

a_i = coil inside radius, cm (except where otherwise noted)
a_0 = coil outside radius, cm (except where otherwise noted)
B_i = intensity of magnetization, gauss
d = diameter, ft or in.
E = coil voltage drop, v
F = force, dynes
F_1,F_2,F_3 = dimensionless magnetic coil factors (Ref. 6)
g = acceleration due to gravity, 980 cm/sec^2
H = magnetic field strength, amp-turn/cm
H_0 = empty space magnetic field strength, amp-turn/cm
H_{eff} = effective magnetic field strength in the vicinity of a finite ferromagnetic body, amp-turn/cm
$\bar{H}$ = dimensionless coil power factor (Ref. 6)
I = current, amp
I_n = gradient coil current required to support a body with a load factor n, amp
J = current density, amp/cm^2
ℓ = coil winding length, cm (unless otherwise noted)
m_b = mass of body, g
M = Mach number
$\bar{M}$ = dimensionless coil power factor (Ref. 6)
n = load factor; total load divided by the body weight
$N/4\pi$ = demagnetization factor of a finite ferromagnetic body
p_0 = settling chamber pressure, mmHg
P = power, w
q = dynamic pressure, psi
r = radial coordinate, cm
Re = Reynolds number based on diameter
U = velocity
V = volume, cm^3
z = axial coordinate, measured positive outward from coil face, cm (unless otherwise noted)
Δz = spacing between Helmholtz coil pair, in.
α = winding efficiency coefficient of coil
ρ_b = mass density of model material, g/cm^3
ρ_c = electrical resistivity, ohm-cm
ϕ = angle between magnetization vector and coil axis, deg

Subscripts and superscripts

$\overline{(\ )}$ = nondimensionalized by a_i
$(\ )_a$ = aerodynamic component
$(\ )_g$ = gravitational component
$(\ )_m$ = magnetic component
$(\ )_r$ = radial component
$(\ )_z$ = axial component

Presented as Paper 68-401 at the AIAA 3rd Aerodynamic Testi g Conference, San Francisco, April 8–10, 1968; submitted June 10, 1968; revision received Feb. 17, 1969. This research was supported by NASA under Grant NsG-86-60 and was performed under the technical cognizance of H. Bankaitis, NASA Lewis Research Center. The research was carried out at the Gas Dynamics Laboratories of the Department of Aerospace Engineering, the University of Michigan, under the direction of J. A. Nicholls and represents part of the Ph.D. thesis. The author gratefully acknowledges the assistance of M. Henderson who was responsible for the design and construction of the electronic components of the control system and who participated in the construction and initial operation of the complete support-and-balance system.

* Associate Professor, Aeronautical and Astronautical Engineering Department. Member AIAA.

1. Introduction

THE development of a one-component, magnetic support-and-balance system for wind-tunnel models was part of an experimental study of sphere drag[1] under flow conditions applicable to the problem of the flow of solid particles in the exhausts of rocket motors using metallized fuels. Such particles experience flows with Mach numbers from the incompressible up to the low supersonic and Reynolds numbers from a few hundred down to values on the order of unity. In addition, these flows are characterized by high freestream turbulence. Although these particles can be approximated by spheres, the effect of large surface roughness must be considered. It was the objective of this study to investigate sphere drag under these flow conditions using a fixed-model experimental technique permitting accurate knowledge and control of the test conditions.

The most obvious experimental technique satisfying this requirement is the continuous wind tunnel. However, the use of this approach to measure sphere drag at low Reynolds numbers has two serious limitations. Foremost is the interference of the model support with the wake flow at Reynolds numbers where the wake is beginning to form. In addition, the very small drag forces result in severe problems in the use of a conventional mechanical drag balance.

A search for a suitable experimental approach suggested the use of a magnetic support-and-balance system in conjunction with a small, continuous wind tunnel. The design and operation of magnetic balance systems are well understood and their application to wind-tunnel testing is not uncommon. The history of development of magnetic support systems for wind-tunnel models has been outlined by Clemens

and Cortner in their bibliography.[2] An excellent view of the state-of-the-art of magnetic support-and-balance systems for wind-tunnel models is provided by Ref. 3.

The magnetic balance solves the problems involved in the use of a mechanical support-and-balance system. First, and obviously, the experiment is free of a physical model support. Second, the practical unit of magnetic support force is the weight of the model alone. Since the ratio of aerodynamic force to model weight increases with decreasing model size, it is found that the use of small models (necessary to achieve small Reynolds numbers) results in high drag forces (in model weight units) and a very sensitive magnetic balance for measuring otherwise very small drag forces.

2. System Design

In selecting a configuration for the magnetic support-and-balance system, the principal criteria were simplicity and low cost. Since, initially, the interest was in drag force only, alignment of the drag and gravity force vectors allowed consideration of a true one-component system. In essence, such a system is a simple extension of the one-component magnetic support system developed by Holmes[4] in 1937.

The attainment of a true one-component system is complicated by the fact that the sphere possesses three degrees of freedom. Even when constrained in the flow direction, the sphere can be perturbed laterally; e.g., by freestream turbulence and/or by an unsteady wake. Holmes[4] showed that it was possible to support a body against the force of gravity with natural horizontal stability, provided that the body was located correctly in the field of the solenoid. However, in his initial experiments on supporting a needle, a provision was made for magnetic damping of horizontal motions. In the center of the wind tunnel, the model is relatively isolated from its surroundings. This sharply reduces the possibility of effective magnetic damping. Thus, a major unknown was whether or not the sphere would remain near the test-section centerline and not be subject to unacceptable horizontal motions.

The support-and-balance system consisted of two major subsystems: 1) the magnetic system and 2) the control system. These systems were designed to be compatible with a vertical, subsonic wind tunnel having a 2-in.-diam test section. The magnetic and control systems are discussed in Secs. 2.1 and 2.2, respectively, below. The calibration and performance of the support-and-balance system are discussed in Sec. 3.

2.1 Magnetic System

The axial magnetic force F_z acting on a ferromagnetic body, located on the axis of a magnetic coil, can be approximated

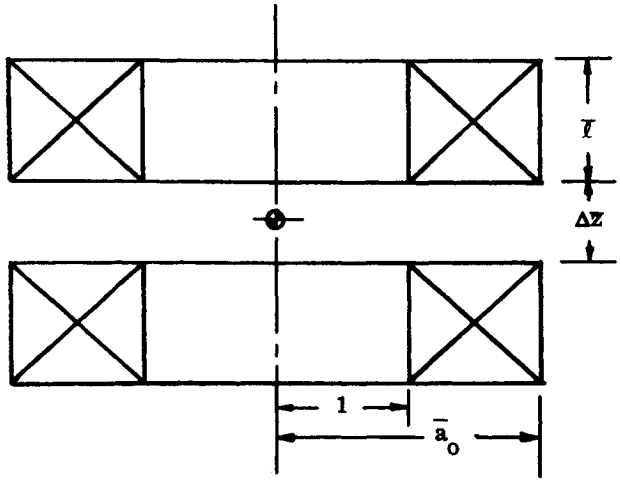

Fig. 1 Geometry of Helmholtz coil pair.

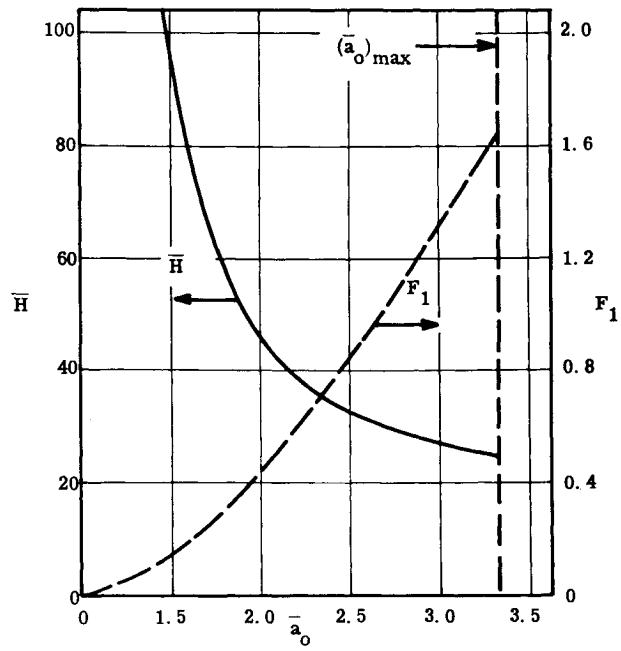

Fig. 2 Helmholtz pair field and power factors.

by the expression

$$F_z \simeq VB_i(\partial H_z/\partial_z)\cos\phi \tag{1}$$

The one-component, support-and-balance system was designed to generate and control this force. If the supported body's intensity of magnetization B_i is held constant, a linear relationship exists between $\partial H_z/\partial z$ and F_z. Because of the very large field strengths required to saturate a spherical body magnetically (resulting in a constant B_i) and because of the very low field gradients needed in the present application, the design of the magnetic system was based on two separate coil systems: one to provide a steady, uniform field to magnetize the body and the other to provide sufficient, controllable field gradient for support of the body.

Field coils; magnetization of a sphere

The uniform magnetic field was produced by a Helmholtz coil pair. The characteristics and design of Helmholtz coils with finite winding areas have been discussed by Franzen.[5] The nondimensional geometry of a typical Helmholtz pair is shown in Fig. 1. Based on Frazen's result, the coil geometry is given by

$$\bar{\ell} = 0.928(\bar{a}_0 - 1) \tag{2a}$$

$$\Delta\bar{z} = 1.428 - 0.428\,\bar{a}_0 \tag{2b}$$

Expressions for axial field strength, and the power required to produce it, on the axis of a coil and at some distance z from the coil face, can be written in the form[6]

$$H_z = \tfrac{1}{2}Ja_iF_1 \tag{3}$$

and

$$P = (4\rho_c/\alpha)a_iH_z^2\bar{H} \tag{4}$$

where F_1 and $\bar{H}$ are nondimensional factors that depend only on the geometry (nondimensionalized by the coil inner radius a_i) of the coil and the axial point z and not on the scale of the configuration. Values of F_1 and $\bar{H}$ are shown in Fig. 2 for the Helmholtz coil pair geometry. It must be noted that the F_1 and H values shown are for one coil only. That is, they can be used to determine the field contribution of one coil alone (one-half of the total field) and the power consumed by that coil.

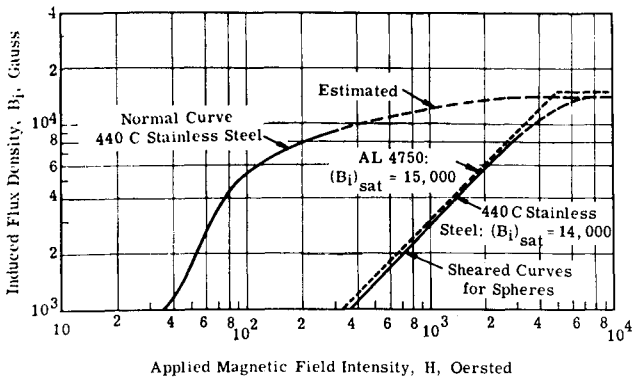

Fig. 3 Material magnetization curves.

Based on considerations of 1) space inside the coil for the test section and the gradient coils, 2) spacing between the coils for the model position detector, and 3) reasonably low power consumption, the geometry selected for the Helmholtz fields coils is as given in Table 1. This geometry gave for the dimensionless field strength and coil power factors, $F_1 = 0.5$ and $\bar{H} = 42$.

The power requirement of field coils is related to the magnetization properties of model material through the field strength required to magnetize the model. The magnetization characteristics of ferromagnetic materials are described by curves relating the intensity of magnetization B_i to the applied field strength H. A number of materials reach magnetic saturation at applied field strengths of a few oersted or less. These materials possess saturated values of B_i in the range from 3000 to 1,5000 gauss. Unfortunately, this performance occurs only in specimens not affected by the magnetic poles set up in the specimens themselves, i.e., rings or infinitely long cylinders. In the case of spheres, the poles are everywhere close to the specimen and have a very strong demagnetizing effect.[7] This effect is described by the relationship

$$H_{\text{eff}} = H_0 - (N/4\pi)B_i \tag{5}$$

where H_{eff} = effective applied field strength, H_0 = applied field strength in the absence of demagnetizing effects, and $(N/4\pi)$ = demagnetization factor = $\frac{1}{3}$, for spheres. Rearranging Eq. (5) for spheres,

$$B_i = 3(H_0 - H_{\text{eff}}) \tag{6}$$

Here, H_{eff} is the field strength as it occurs in a normal magnetization curve for an infinitely long specimen. One observes that, until H_{eff} becomes very high (at or above saturation for easily magnetized ferromagnetics), B_i is approximated by the relation

$$B_i \simeq 3H_0 \tag{7}$$

Thus, for spheres, the use of easily magnetized (and expensive) ferromagnetics generally is not warranted and the magnetization obtained will be nearly independent of the sphere material.

This demagnetization effect made the problem of material selection and model manufacture a trivial one. Precision ball bearings, made of weakly magnetic Type 440C stainless steel, are commercially available. The sheared (for a spherical specimen) magnetization curve for this material is compared with its normal magnetization curve and the sheared curve for easily magnetized (an H_{eff} of about 10 oersted at saturation) Allegheny Ludlum electrical steel 4750 in Fig. 3.

The field coils were wound with $\frac{1}{4}$-in. o.d. by 0.030-in.-wall copper tubing with a $\frac{1}{32}$-in.-thick polyvinyl chloride (PVC) insulating sheath, giving a winding efficiency factor α of about 0.2. This tubing was suitable for use at pressures up to about 500 psi and temperatures up to about 200°F.

Table 1 Helmholtz coil geometry

$a_i = 3$ in.	
$\bar{a}_0 = 2.09$;	$a_0 = 6.27$ in.
$\bar{\ell} = 1.0$;	$\ell = 3.0$ in.
$\Delta\bar{z} = 0.54$;	$\Delta z = 1.62$ in.

The calculated electrical characteristics of the Helmholtz coil pair (electrically connected in series) are given in Table 2. These values fell well within the capabilities of the Gas Dynamics Laboratories' d.c. power supply.

Cooling water was supplied by a 500 psi, 2 gpm pump. This performance matched the 500 psi pressure drop across each coil at a flow rate of 1 gpm; the coils were connected in parallel for cooling purposes. With this water-flow rate and a power input of 34 Kw (corresponding to a 3000 oersted field) the outlet water temperature was calculated to be about 165°F. This was taken as a working maximum to insure that the PVC insulation did not exceed its 200°F maximum working temperature. This situation limited the maximum field to 3000 oersted (corresponding to a B_i of a sphere of about 8300 gauss).

Gradient coil

The gradient coil system was designed to meet the two objectives of low input power and radial stability of the model. It can be shown[6] that the power required for a gradient coil, supporting a load n times the weight of the ferromagnetic body, can be written as

$$P = 3.842 \times 10^8(n^2/\alpha)\rho_c a_i^3(\rho_b/B_i)^2\,\bar{M} \tag{8}$$

The radial stability derivative for the body is given by

$$(1/m_b)(\partial F_r/\partial_r) = -4.9 \times 10^2(n/a_i)(F_3/F_2) \tag{9}$$

and the axial magnetic force acting on the body can be written as

$$F_z = -0.05VB_iJF_2\cos\phi \tag{10}$$

$\bar{M}$, F_2, and F_3/F_2 are nondimensional magnetic coil factors that are determined by the coil geometry, but not its scale. In addition, F_2 is related to the field gradient through the equation

$$\partial H_z/\partial_z = -\tfrac{1}{2}JF_2 \tag{11}$$

The evaluation of these factors is discussed in detail in Ref. 6.

In general, there are two axial positions, relative to the face of the coil, where the field gradient is of the correct magnitude to produce the desired magnetic force. However, the equation for the radial stability derivative above shows that the ratio F_3/F_2 must be positive and it can be shown that positive values of F_3/F_2 occur only near the coil face and become more positive as the coil face is approached. In a magnetic support system such as this, radial and axial stability derivatives of the supported body are found to be mutually exclusive; i.e.,

$$\partial F_r/\partial r = -\tfrac{1}{2}\partial F_z/\partial_z \tag{12}$$

Thus, a design based on achieving natural stability results in a system that is axially unstable. Overcoming this axial in-

Table 2 Helmholtz coil electrical characteristics

H_z, oersted	2000	3000
P, Kw	15	34
J, amp/in.^{2}	2700	4000
I, amp	260	390
E_{total}, v	58	87

Table 3 Gradient coil geometry

a_i = 1.5 in.
$\bar{a}_0$ = 1.5; a_0 = 2.25 in.
$\bar{\ell}$ = 0.5; ℓ = 0.75 in.
$\bar{z}$ = the practical minimum depending on the model diameter

stability is an added requirement for the control system described in Sec. 2.2 below.

The gradient coil was designed to meet the requirements of positive model radial stability, low input power, and the available space. The design selection was based on the parametric study of the dimensionless solenoid factors reported in Ref. 6. The resulting geometry is given in Table 3. If it is assumed that $\bar{z} \simeq 0.1$, the corresponding coil factors are $F_1 \simeq 0.18$, $F_2 \simeq 0.11$, $F_3/F_2 \simeq 2$, and $\bar{M} \simeq 170$, where Eq. (3) relates F_1 to the magnetic field produced by the coil.

The field produced by the gradient coil changes with the load on the suspended model and, hence, the magnetization of the unsaturated model will change with the load. This upsets the desired linearity between field gradient and magnetic force. This effect can be substantially reduced by using two gradient coils; one above and one below the model. In this configuration, the field gradients are additive, but the fields tend to cancel each other. The theoretical distributions of F_1 and F_2 (proportional to the field and field gradient, respectively) along the coil axis are compared in Fig. 4 for the single and double coil configurations.

The use of two coils reduces the power required by each coil by a factor of about four (the total input power to the gradient coils decreases by about one half). This effect substantially reduces the heating of the coils; in the present design this reduction eliminated the requirement for cooling of the coils.

The disadvantage of the two-coil configuration lies in a decrease in radial stability. Even though the contributions to F_2 and F_3 are additive near the face of the primary coil, the stability-related ratio F_3/F_2 is decreased everywhere between coils. This decrease, shown in Fig. 4, resulted in about a 40% reduction in radial stability in the present design.

In the interest of reducing both the variation of B_i with sphere drag variation and the coil heating, the two-coil configuration was selected for the present design. The coils were wound from no. 20 copper magnet wire, giving a resistance of about 4.5 ohms/coil and a winding efficiency of about 0.7. On this basis, the electrical requirements of the gradient coil pair (connected in series) for supporting a steel sphere (n = 1) were as given in Table 4.

The relationship between model load and the required current density in the coil is given by the equation

$$J = -1.96 \times 10^4 (n\rho_b / B_i \cos\phi)(1/F_2) \qquad (13)$$

The over-all performance criterion for the support system was the support of a total load of four times the model weight; i.e., n = 4. On this basis, the maximum electrical requirement for the gradient coil pair were I = 3.8 amp, E = 34 v, and P = 130 w.

2.2 Magnetic Force Control System

As pointed out previously, the magnetic support-and-balance system was based on the separation of the model

Table 4 Gradient coil electrical characteristics

Axial field H_z due to the field coils, oersted	2000	3000
Spherical model magnetization B_i, gauss	5700	8300
Gradient coil power, w/coil	4.0	1.8
Gradient coil current, amp	0.95	0.63
Voltage drop across the coil pair, v	8.5	5.7

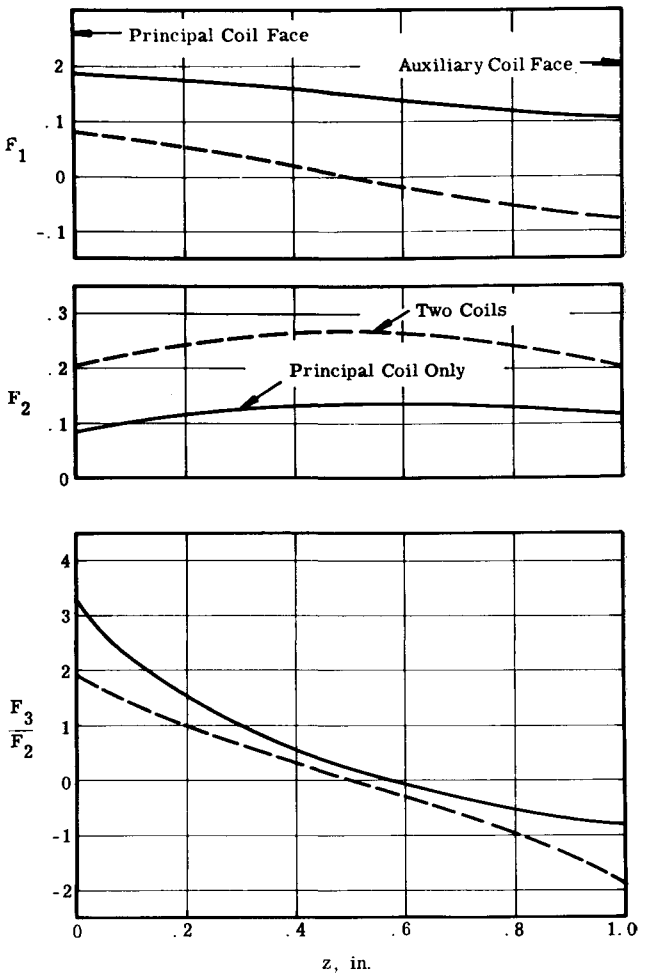

Fig. 4 Solenoid factor distributions for one and two gradient coil systems.

magnetization B_i and the field gradient $\partial H_z/\partial_z$ factors in the magnetic force equation, Eq. (1). Introducing Eq. (11) and noting that for a given coil the winding current density J is proportional to the conductor current I, the magnetic force equation can be written as

$$F_z \propto VB_iIF_2 \qquad (14)$$

Thus, F_z varies linearly with I provided that both B_i and F_2 are held constant. F_2 depends only on the geometry of the system and, for a given set of gradient coils, only on the axial position of the model relative to the coils (see Fig. 4). This suggests that, in addition to providing control of the magnetic force so that the model is stably supported, it is desirable for the control system to keep the model fixed in space. The control system was a closed loop, feedback system† that included, in addition to the magnetic body and the gradient coils, 1) a model position detector, 2) a compensator, and 3) a gradient coil current controller.

Model position detector

The model position detector was designed to sense the position of the model by a light beam splitting technique and to generate a voltage signal proportional to the model's deflection from some desired position. The arrangement of the detector is sketched in Fig. 5. A photograph of the sensing unit is shown in Fig. 6. Collimated light from a flashlight

† The design and construction of the control system was done by M. Henderson. A more detailed discussion of the system is presented in Ref. 8.

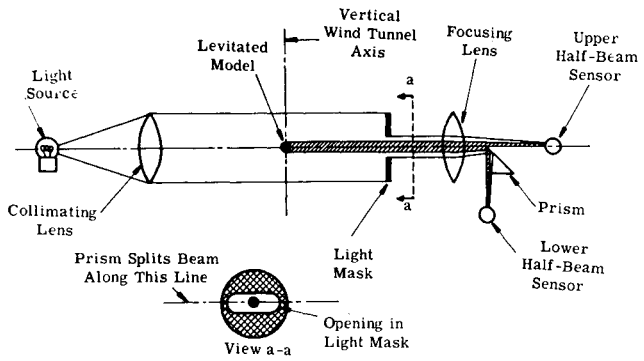

Fig. 5 Sketch of model position detector configuration.

bulb was projected through the wind-tunnel test section windows, and fell on the light mask. The light that passed the mask was refocused and split horizontally by a 45° prism. The two beam halves fell on light sensors (photovoltaic cells) located near the focal points. These sensors were current sources and their output was a linear function of the light energy incident on the sensor. The output circuits of the sensors were arranged so that the net detector output voltage was zero when each sensor received the same light input.

In operation, the detector was adjusted so that the net output voltage was zero when a supported sphere was located so that its shadow was split in half by the prism; this was the null position for the sphere. Motion of the sphere from its null position produced a net voltage output that was roughly proportional to the extent of the motion; the voltage polarity indicated the direction of motion.

The opening in the light mask was slightly greater than the sphere diameter in height and was three or more diameters in width. This horizontal dimension permitted the sphere to move laterally with negligible effect on the vertical control performance.

Compensator

The compensator was essentially a small analog computer operating on the voltage signal coming from the model position detector. The compensator provided error-rate control; i.e., its output was related to the magnitude and sign of both the input signal and its first time derivative. The compensator was capable of providing sufficient positive stability to the entire control loop to compensate for the (vertical motion) instability of model/magnetic force portion of the loop.

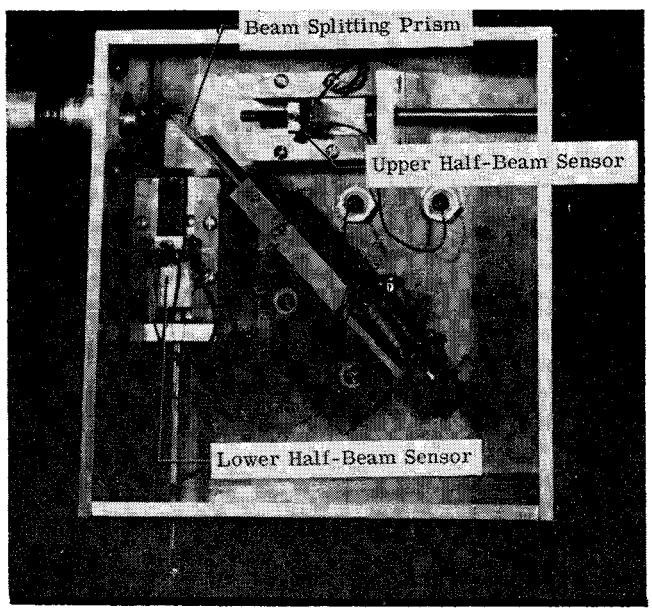

Fig. 6 Photograph of sensor unit.

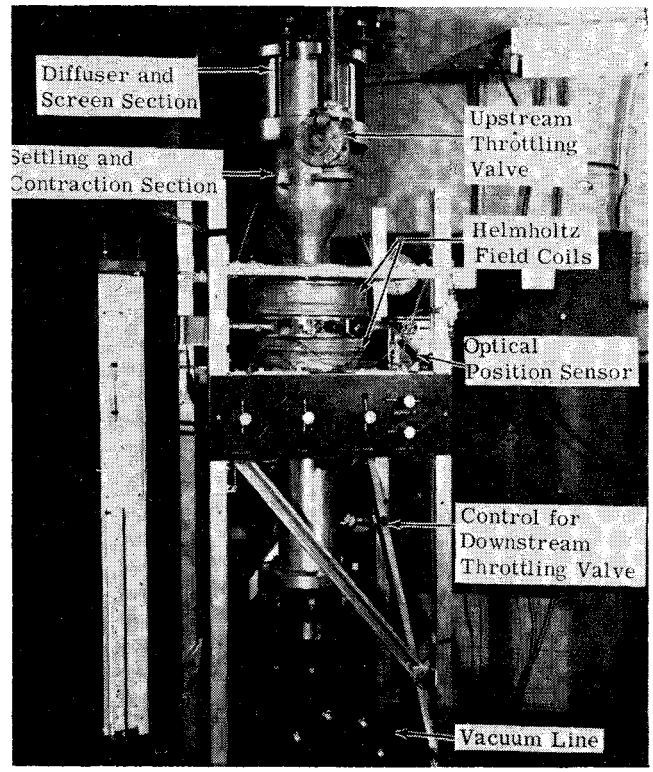

Fig. 7 Photograph of wind tunnel.

Under steady-state conditions, a simple error-rate controller has an output that is directly proportional to the input signal. This characteristic would produce model sag (movement toward the principal coil face) as the drag load increases and upset the linear relationship between F_z and I, since F_2 would be a function of F_z. This effect was reduced by introducing an integrating circuit into the compensator. The output of the integrator was the time integral of the input and was summed together with the error and the error rate so that steady-state errors always tended toward zero. The time constant of the integrator was about 0.1 sec. This was about two orders of magnitude greater than the time constant of the rest of the control loop and hence the integrator did not affect system response to rapidly varying model loads.

Gradient coil current controller

The voltage output of the compensator was used as the input to the gradient coil current controller, a solid-state power amplifier. The power was supplied by a 48 v, 6 amp, d.c. power supply. The controller had a rise time of less than 10 μsec, and hence did not influence the over-all response time of the control system.

3. Calibration and Performance

A photograph of the wind tunnel with the support-and-balance system installed is presented in Fig. 7. Details of the geometric arrangement of the coils, wind-tunnel test section, and the model are shown in Fig. 8. Also shown are the directions of the induced magnetization, the field gradient, and the forces acting on the model; positive z is taken upward, measured from the upper face of the lower or principal gradient coil. Because of space requirements for the model position detector and the field coil arbor end plates, the Helmholtz coils were separated by 2 in. rather than by the design spacing of 1.62 in. The gradient coils were spaced 1 in. apart with the lower coil face slightly below the position detector axis.

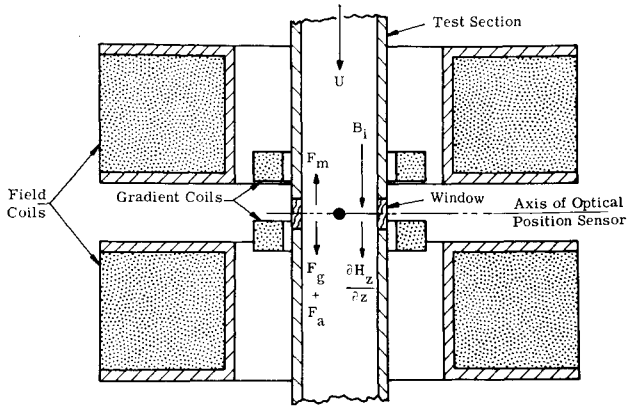

Fig. 8 Sketch of magnetic coils and test section assembly.

Axial magnetic field strength measurements showed that the Helmholtz coils generated 7.55 oersted/amp at their geometric center. Thus, a 2000 oersted field required a current of 265 amp, compared to the design value of 260 amp. The voltage drop across the coils, at this current, was about 60–65 v, compared to the design estimate of 58 v. No detectable field variation was found within a 1-in. radius of the center of the coils, verifying the effectiveness of the Helmholtz design and justifying the greater than design separation between the coils.

The axial magnetic field, due to the gradient coils, in the vicinity of the model was found to be about 25 oersted/amp, opposing the field due to the Helmholtz coils. This field produced a decrease in B_i of about 1%/g of model load for a Helmholtz field of 2000 oersted or about 0.5%/g for a 3000 oersted field.

A static load calibration was used to verify the linearity between the force on the model and the gradient coil current. It should be noted that the system was calibrated automatically at one point each time it was used. Each test was begun by suspending the model alone in still air. This determined the coil current required to produce a magnetic force equal to one model weight, i.e., 1 g or $n = 1$.

The calibration procedure was as follows. A fine thread, with a loop at one end, was cemented to a sphere and the whole assembly weighed in a precision balance, as was the sphere before attaching the thread. Then the sphere with the attached thread was magnetically suspended. Finally, carefully weighed pieces of nonmagnetic wire were hooked to the loop to "load" the system. The practical unit of weight in this system is the weight of the sphere alone. Therefore, the load factor n (the total weight of the sphere, string, cement, and attached weights divided by the weight of the sphere alone) was taken as the loading unit. Figure 9 presents the results of two typical system calibrations in the form of the gradient coil current ratio, $(I_n - I_{n0})/I_{n=1}$ where I_{n0} is the current required to support the sphere plus thread and cement, as a function of incremental load factor, $n - n_0$.

These results show a small nonlinearity in the system. Part of this is due to the 1% decrease in B_i/g of load referred to above. The remainder is due to a nonlinear model sag under load, resulting in a decreasing field gradient with load; an indication of the inability of the integrating circuit to remove the entire steady-state position error due to loading. This sag can be decreased by increasing the gain of the compensator. However, the system became unstable at high gains; the results presented in Fig. 9 are for the highest practical gain setting for each sphere size.

Two simple tests were made to demonstrate the dynamic response characteristics of the system. First, a small nonmagnetic weight was dropped onto a suspended sphere. This weight bounded off the sphere and effectively produced an impulse load input to the system. Oscilloscope studies of the position detector output showed that the system had good

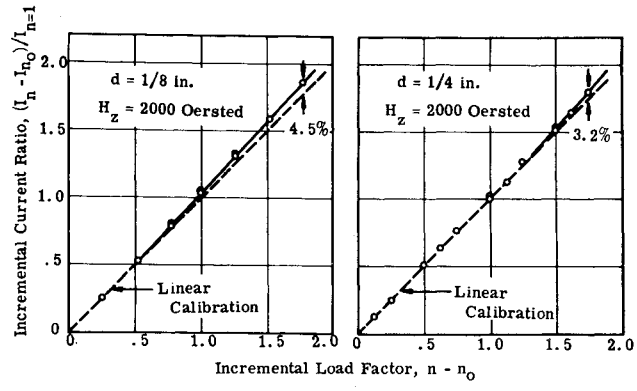

Fig. 9 Calibration of magnetic balance.

dynamic stability with a natural frequency (with the $\frac{1}{4}$-in.-diam sphere used in this test) of about 26 cps. The oscillations damped out in about 100 msec. and the sphere returned to its initial position in about 135 msec. In the second test, a $\frac{1}{8}$ g wt was dropped onto the loading loop of a suspended sphere. This produced a step load input. In this case, the sphere motion was arrested in about 100 msec. and the integrator required about another 250 msec. to return the sphere to its initial position. Again, the system exhibited satisfactory dynamic response.

The sphere drag data obtained with this support-and-balance system are discussed in Refs. 1 and 9. Some typical data from this investigation are shown in Fig. 10. This figure shows the dimensionless drag force (load factor n-1) vs the tunnel stagnation pressure for $M = 0.16$. The drag force, n-1, was determined from the measured gradient coil current on the basis of the relationship n-1 = [(I) wind-on/(I) wind-off]-1. Figure 10 also shows the drag force reduced by the dynamic pressure. This ratio, $(n\text{-}1)/q$, is proportional to the drag coefficient. These data cover the Reynolds

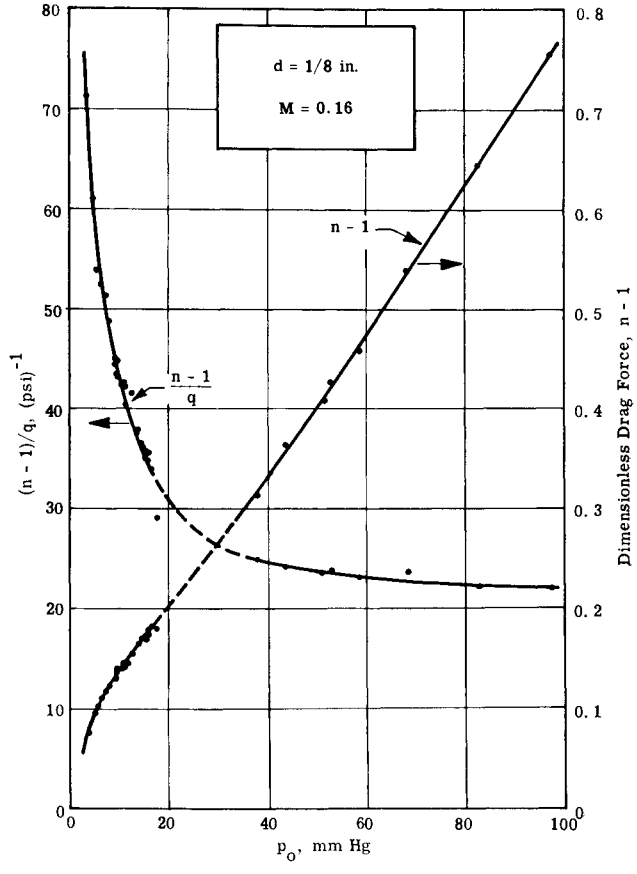

Fig. 10 Typical sphere drag data.

number range from about 50 to 1500. The data shown in Fig. 10 are typical with respect to the small scatter and good repeatability that was achieved with the system.

The sensitivity of this system was demonstrated by measuring the drag on $\frac{1}{16}$-in.-diam spheres at values of Re down to about 25. At this test condition, the drag force was about 4 mg.

Radial stability was found to be an important factor in the operation of the support-and-balance system. Below a Reynolds number of about 300 ($p_0 < 18$ mmHg in Fig. 10), the flow about the sphere was essentially steady and the model was subjected to negligible lateral disturbances (for a low-turbulence freestream). Under these conditions, the models were found to remain almost motionless at the test-section center. At higher Reynolds numbers ($Re > 300$), the unsteady separated flow at the rear of the sphere and the wake produced large lateral force fluctuations. These fluctuations caused the model to oscillate laterally; sometimes with sufficient amplitude to drive the model outside the position detector's light beam, resulting in loss of the model. Under this condition of fluctuating lateral forces, the natural radial stability of the system was insufficient. In spite of this, it was possible to obtain good drag data at values of Re up to 4000; the limitation was in wind-tunnel operation and not in the magnetic support-and-balance system.

4. Conclusions

The practicality and effectiveness of a one-component, magnetic support-and-balance system in the study of sphere drag have been demonstrated. This technique was found to be particularly valuable at low sphere Reynolds numbers where the use of small spheres is advantageous. Under these conditions, the magnetic support system eliminates support interference effects and the balance sensitivity increases as the sphere size (and the corresponding drag force) decreases.

The one-component system provided model position control only along the wind axis. Thus, satisfactory operation depended on the natural radial stability of the system to restrain the model in the two lateral degrees of freedom. The one-component system was found to be completely satisfactory at Reynolds numbers below 300 where flow about the sphere produces negligible lateral force fluctuations. However, at higher Reynolds numbers, the unsteady separated flow at the rear of the sphere and the fluctuating wake were found to produce fluctuating lateral forces that caused substantial lateral motion of the sphere. In some cases, this motion was sufficient to cause loss of the model. For such test conditions, support operation would be substantially improved by the addition of controlled lateral stability to aid in holding the model in a fixed position.

Finally, the simplicity and relatively low cost of the one-component system were demonstrated. With a magnetizing field of 2000 oersted, it was possible to support stainless steel spheres with gradient coil currents of about 1 amp/g of force on the sphere. Thus, the gradient coil current controller was required to handle at most a few amperes. Because of the larger demagnetization effect of the spherical shape, the 2000 oersted field was able to magnetize the ferromagnetic spheres only to about 40% of the saturated value. The availability of a 7000 oersted field would have saturated the spheres magnetically and reduced the gradient coil current requirement by about 60%.

References

[1] Sivier, K. R., "Subsonic Sphere Drag Measurements at Intermediate Reynolds Numbers," Ph.D. thesis, Univ. of Michigan, 1967.

[2] Clemens, P. L. and Cortner, A. H., "Bibliography: The Magnetic Suspension of Wind Tunnel Models," Rept. AEDC-TDR-63-20, Feb. 1963, U.S. Air Force.

[3] Daum, F. L., ed., "Summary of ARL Symposium on Magnetic Wind Tunnel Model Suspension and Balance Systems," OAR Rept. ARL 66-0135, July 1966, U.S. Air Force.

[4] Holmes, F. T., "Axial Magnetic Suspensions," *The Review of Scientific Instruments*, Vol. 8, Nov. 1937, p. 444.

[5] Franzen, W., "Generation of Uniform Magnetic Fields by Means of Air-Core Coils," *The Review of Scientific Instruments*, Vol. 33, No. 9, Sept. 1962, p. 933.

[6] Sivier, K. R., "Magnetic Field Properties Related to the Design of a One-Component Magnetic Support-and-Balance System," NASA CR-1352, May 1969, Univ. of Michigan.

[7] Bozorth, R. M., *Ferromagnetism*, Nostrand, 1951, pp. 1–11 and 845–849.

[8] Sivier, K. R. and Henderson, M., "One-Component Magnetic Support-and-Balance System for Measuring Sphere Drag," NASA CR-1353, May 1969, Univ. of Michigan.

[9] Sivier, K. R., "Subsonic Sphere Drag Measurements at Intermediate Reynolds Numbers," NASA CR-1392, July 1969, Univ. of Michigan.